

# Low-energy behavior of $E2$ strength functions

R. Schwengner

*Helmholtz-Zentrum Dresden-Rossendorf, 01328 Dresden, Germany*

(Dated: March 5, 2022)

Electric quadrupole strength functions have been deduced from averages of a large number of  $E2$  transition strengths calculated within the shell model for the nuclides  $^{94}\text{Mo}$  and  $^{95}\text{Mo}$ . These strength functions are at variance with phenomenological approximations as provided by the Reference Input Parameter Library RIPL-3 for calculations of reaction rates on the basis of the statistical model.

PACS numbers: 25.20.Dc, 21.10.Tg, 21.60.Jz, 23.20.-g, 27.50.+e

## I. INTRODUCTION

Photonuclear reactions and the inverse radiative-capture reactions, in particular radiative neutron capture, play a central role in the synthesis of heavy elements in various stellar environments [1, 2] and also in next-generation nuclear technologies, such as the transmutation of long-lived nuclear waste [1, 3]. As these reactions include the excitation and deexcitation of nuclear states at high excitation energy and large level density, the so-called quasicontinuum of states, the statistical reaction theory is the basis for calculations of rates of these reactions. A critical input to such calculations is photon strength functions that describe average electromagnetic transition strengths. Modifications of the strength functions can change reaction rates considerably. For example, modifications of the electric dipole strength function have drastic consequences for the abundances of elements produced via neutron capture in the r-process occurring in violent stellar events [4].

In the calculations using statistical codes (e.g. TALYS [5]), usually electric dipole ( $E1$ ), magnetic dipole ( $M1$ ), and electric quadrupole ( $E2$ ) strength functions are taken into account. In the energy range below the particle-separation energies, which is relevant for radiative capture reactions, the dipole strength function is dominated by the low-energy tail of the isovector electric giant dipole resonance (GDR). The GDR is considered as a collective vibration of the neutron system against the proton system. The damping of the vibration is described by a Lorentz curve as a function of the photon energy [6–8]. Combinations of two or three Lorentz curves are used to describe the double or triple humps of the GDR caused by quadrupole and triaxial deformation of the nuclei [9–11]. Such a parametrization gives a good description of the experimental photoabsorption cross section  $\sigma_\gamma = 3(\pi\hbar c)^2 E_\gamma f_1(E_\gamma)$  of nuclei in the ground state. The so-called Brink-Axel hypothesis [6, 7] expresses the assumption that the strength function does not depend on the excitation energy. This means that the strength function describing the absorption of photons is identical with the one for the emission of photons from highly excited states, for example following neutron capture. The Generalized Lorentzian (GLO) [12] includes a correction to the Standard Lorentzian (SLO) [6, 7], which accounts

for the temperature of the nucleus emitting the photons. The magnetic dipole ( $M1$ ) contribution to the strength function used in statistical-reaction codes is also approximated by a Lorentz curve with parameters derived from systematics [8]. This curve accounts for the spin-flip mode that appears around 8 MeV [13].

In several experiments, deviations from the phenomenological strength functions have been observed. A bump of the  $M1$  strength around 3 MeV in deformed nuclei is generated by the scissors mode, which is interpreted as a small-amplitude rotation of the neutron system against the proton system [13]. After it had been well established in the absorption spectra of the ground state, it was recently also identified in the emission from highly excited states [14].

An enhancement of  $E1$  strength has been found in the energy region from about 6 MeV up to the respective neutron-separation. This additional strength on top of the low-energy tail of the GDR is considered as the pygmy dipole resonance (PDR) which is interpreted as the vibration of excessive neutrons against the symmetric  $N = Z$  neutron-proton system. A review of experimental studies of the PDR can be found in Ref. [15].

In contrast to the Lorentz curves used for the  $E1$  and  $M1$  strength functions, which decrease toward  $E_\gamma = 0$ , an increase of the dipole strength below 3 MeV toward low  $\gamma$ -ray energy has been found in several nuclides in the mass range from  $A \approx 50$  to 100, such as  $^{56,57}\text{Fe}$  [16],  $^{60}\text{Ni}$  [17], various Mo isotopes [18], and  $^{105,106}\text{Cd}$  [19]. Neither of these measurements were able to distinguish clearly between  $E1$  and  $M1$  strength, although an indication for an  $M1$  character of the low-energy enhancement was discussed for the case of  $^{60}\text{Ni}$  [17]. In an analysis of  $M1$  strength functions deduced from shell-model calculations of a large number of transitions in the isotopes  $^{90}\text{Zr}$ ,  $^{94}\text{Mo}$ ,  $^{95}\text{Mo}$ , and  $^{96}\text{M}$  [20] we showed that the low-energy enhancement of the dipole strength can be explained by  $M1$  transitions between many close-lying states of all considered spins located above the yrast line in the transitional region to the quasi-continuum of nuclear states. Inspecting the wave functions, one finds large  $B(M1)$  values for transitions between states containing a large component of the same configuration with broken pairs of both protons and neutrons in high- $j$  orbits. The large  $M1$  matrix elements connect con-

figurations with the spins of high- $j$  protons re-coupled with respect to those of high- $j$  neutrons to the total spin  $J_f = J_i, J_i \pm 1$ .

In an alternative work the low-energy enhancement could be described by  $E1$  strength generated by the thermal coupling of quasiparticles to the continuum of unbound states [21]. This effect appears at temperatures above 1.4 MeV, whereas experimentally deduced values and values predicted by the constant-temperature and Fermi-gas models are below 1.0 MeV [18, 22].

For the  $E2$  strength function a Lorentz curve is recommended as well in the RIPL-3 reaction data base [23] with the following parameters: energy of the maximum  $E_{\max} = 63A^{-1/3}$  MeV, width  $\Gamma = 6.11 - 0.021A$  MeV, and maximum of the corresponding cross section  $\sigma_{\gamma, \max} = 0.00014Z^2E_{\max}A^{-1/3}\Gamma^{-1}$  mb. The Lorentz function in combination with the factor  $E_{\gamma}^{-2L+1}$  produces an unrealistic pole at  $E_{\gamma} = 0$ . An experimental test of the real behavior of the  $E2$  strength function at low transition energy has not been feasible so far. However, model calculations may gain information about the  $E2$  strength function at low energy. As the shell-model calculations just mentioned were successful in describing the low-energy enhancement of the  $M1$  strength observed in various experiments [20], these calculations are expected to predict also the low-energy behavior of the  $E2$  strength functions in the considered nuclei near  $N = 50$ .

## II. SHELL-MODEL CALCULATIONS

The present work presents shell-model calculations of  $E2$  transition strengths in  $^{94}\text{Mo}$  and  $^{95}\text{Mo}$ . The calculations were performed by means of the code RITSSCHIL [24] using a model space composed of the  $\pi(0f_{5/2}, 1p_{3/2}, 1p_{1/2}, 0g_{9/2})$  proton orbits and the  $\nu(1p_{1/2}, 0g_{9/2}, 1d_{5/2})$  neutron orbits relative to a  $^{66}\text{Ni}$  core. The configuration space was tested in detail in earlier shell-model studies of nuclei with  $N = 46 - 54$  [25–39] and was found appropriate for the description of level energies as well as  $M1$  and  $E2$  transition strengths in nuclides around  $A = 90$ . As a further test, a comparison of the energies of yrast and yrare levels in  $^{94}\text{Mo}$  and  $^{95}\text{Mo}$  from the present calculation with the experimental ones shows an agreement within 300 keV.

The calculations included states with spins from  $J = 0$  to 10 for  $^{94}\text{Mo}$  and from  $J = 1/2$  to  $21/2$  for  $^{95}\text{Mo}$ . Two protons were allowed to be lifted from the  $1p_{3/2}, 1p_{1/2}$  orbits to the  $0g_{9/2}$  orbit and two neutrons from the  $0g_{9/2}$  orbit to the  $1d_{5/2}$  orbit. This resulted in configuration spaces with dimensions of up to about 16000. For each spin the lowest 40 states were calculated. The reduced transition probabilities  $B(E2)$  were calculated for all transitions from initial to final states with energies  $E_f < E_i$  and spins  $J_f = J_i, J_i \pm 1, J_i \pm 2$ . For the minimum and maximum  $J_i$ , the cases  $J_f < J_i$  and  $J_f > J_i$ , respectively, were excluded. This resulted in more than 36000  $E2$  transitions for each parity  $\pi = +$  and  $\pi = -$ ,

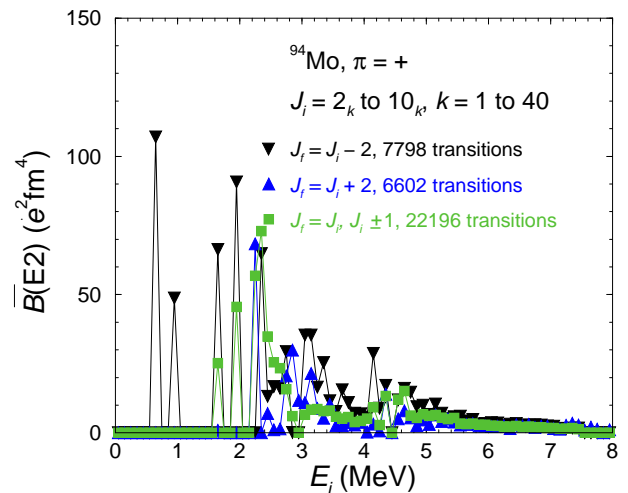


FIG. 1: (Color online) Average  $B(E2)$  values in 100 keV bins of excitation energy calculated for positive-parity states in  $^{94}\text{Mo}$ .

which were sorted into 100 keV bins according to the excitation energy of the initial state  $E_i$  or the transition energy  $E_{\gamma} = E_i - E_f$ . The average  $B(E2)$  value for one energy bin was obtained as the sum of all  $B(E2)$  values divided by the number of transitions within this bin. Effective charges of  $e_{\pi} = 1.5e$  and  $e_{\nu} = 0.5e$  were applied.

## III. RESULTS

Average calculated  $B(E2)$  values in 100 keV wide energy bins of initial excitation energy of positive-parity and negative-parity states in  $^{94}\text{Mo}$  are shown in Figs. 1 and 2, respectively. The  $B(E2)$  values are separately shown for transitions with  $J_f = J_i - 2$ ,  $J_f = J_i + 2$ , and  $J_f = J_i, J_i \pm 1$ .

In Fig. 1, the peak at 0.65 MeV (energy bin from 0.6 to 0.7 MeV) arises from the  $2_1^+ \rightarrow 0_1^+$  transition. The calculated transition strength of  $B(E2) = 107 e^2\text{fm}^4$  is considerably smaller than the experimental value of  $B(E2) = 406(9) e^2\text{fm}^4$  [40]. This holds also for the  $4_1^+ \rightarrow 2_1^+$  transition that dominates the peak at 0.95 MeV. Its calculated value of  $B(E2) = 49 e^2\text{fm}^4$  has to be compared with the experimental value of  $B(E2) = 660(102) e^2\text{fm}^4$  deduced from Coulomb excitation [40]. This comparison shows that collective contributions to the lowest-lying (yrast) states are not fully accounted for in the present configuration space. On the other hand, the calculated value of  $B(E2, 4_2^+ \rightarrow 2_1^+) = 147 e^2\text{fm}^4$ , that predominates in the peak at 1.95 MeV, fits exactly the experimental value of  $B(E2, 4_2^+ \rightarrow 2_1^+) = 147(23) e^2\text{fm}^4$ . This transition connects a non-yrast  $4^+$  state containing the main configuration  $\pi(0g_{9/2}^2)\nu(1d_{5/2}^2)$  with the  $2^+$  yrast state including mainly the configuration  $\nu(1d_{5/2}^2)$ . The configuration  $\pi(0g_{9/2}^2)\nu(1d_{5/2}^2)$  of two active proton and two active neutron high- $j$  orbits is found to be the dominat-

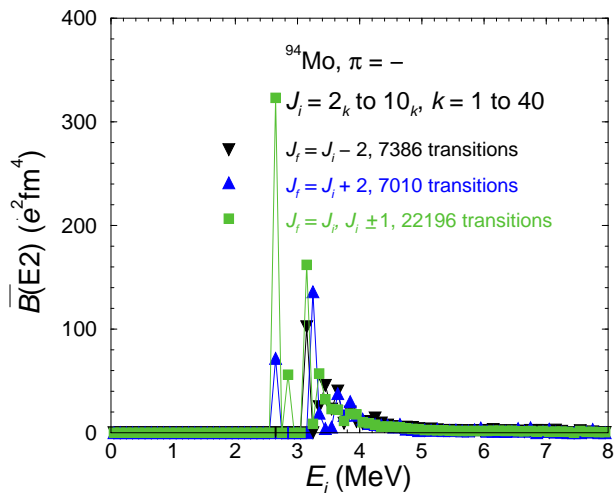


FIG. 2: (Color online) As Fig. 1, but for negative-parity states.

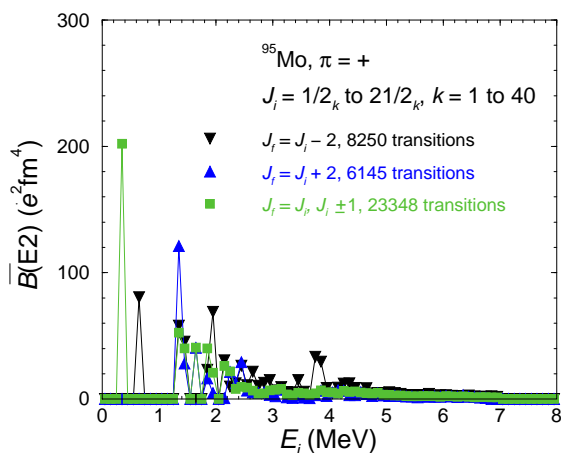


FIG. 3: (Color online) Average  $B(E2)$  values in 100 keV bins of excitation energy calculated for positive-parity states in  $^{95}\text{Mo}$ .

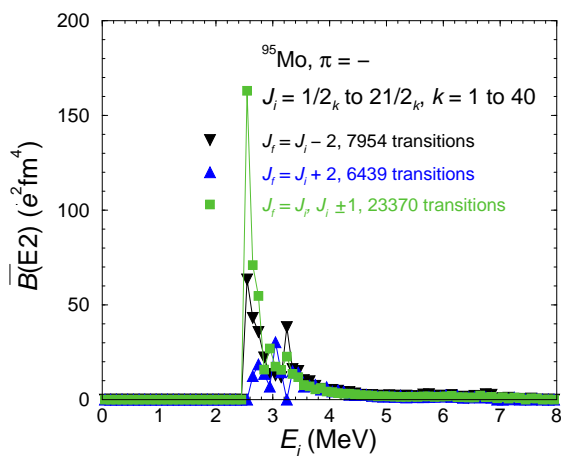


FIG. 4: (Color online) As Fig. 1, but for negative-parity states.

ing configuration in the many close-lying states above the yrast line which are connected by  $M1$  transitions of large strengths [20]. The  $E2$  transitions between states with  $J_f = J_i, J_i \pm 1$  represent admixtures to those  $M1$  transitions. As the states with the predominating four-particle configuration contain little collectivity, the magnitudes of the calculated  $B(E2)$  values between them are considered more realistic than those of the stretched  $E2$  transitions between low-spin yrast states, which is demonstrated by the  $B(E2, 4_2^+ \rightarrow 2_1^+)$  value just mentioned. The lowest states linked by a strong  $M1$  transition are the  $2_3^+$  and  $2_1^+$  states. The calculated  $B(E2, 2_3^+ \rightarrow 2_1^+)$  value of  $87 e^2\text{fm}^4$  compares with an experimental value of  $126(76) e^2\text{fm}^4$  [40].

The distributions at higher  $E_i$  from about 2.5 to 5.5 MeV include contributions from transitions between many states with various spins. The  $B(E2)$  values generally decrease with increasing excitation energy, which is also found for the experimental values compiled in Ref. [40]. In Fig. 2, the peaks at 2.65 and 3.15 MeV are dominated by the  $E2$  admixtures to the  $5_1^- \rightarrow 4_1^-$  and  $5_2^- \rightarrow 4_2^-$  transitions. The  $B(E2)$  distributions for the negative-parity states start at higher excitation energy and decrease faster toward higher energy in comparison with the ones for positive parity.

The values calculated for  $^{95}\text{Mo}$ , shown in Figs. 3 for positive-parity states and in Fig. 4 for negative-parity states, display a similar behavior. In Fig. 3, the peak at 0.35 MeV is caused by the  $E2$  admixture to the  $3/2_1^+ \rightarrow 5/2_1^+$  transition. The calculated value of  $B(E2) = 202 e^2\text{fm}^4$  compares with the experimental value of  $B(E2) = 554(28) e^2\text{fm}^4$  [41]. The peak at 0.65 MeV corresponds to the value of  $B(E2, 9/2_1^+ \rightarrow 5/2_1^+) = 81 e^2\text{fm}^4$  compared with an experimental value of  $B(E2, 9/2_1^+ \rightarrow 5/2_1^+) = 291(15) e^2\text{fm}^4$  [41]. Again, the calculated  $B(E2)$  values of transitions between yrast states underestimate the experimental values. In Fig. 4, the peak formed by the values at 2.55, 2.65, and 2.75 MeV in the distribution of values with  $J_f = J_i, J_i \pm 1$  is caused by the  $B(E2)$  strengths of the  $3/2_1^- \rightarrow 5/2_1^-$ ,  $7/2_1^- \rightarrow 5/2_1^-$ ,  $7/2_2^- \rightarrow 5/2_1^-$ , and  $5/2_2^- \rightarrow 3/2_1^-$  transitions. Main contributions to the peak formed at the same energies in the distribution of  $J_f = J_i - 2$  transitions arise from several  $7/2^- \rightarrow 3/2^-$ ,  $9/2^- \rightarrow 5/2^-$ ,  $11/2^- \rightarrow 7/2^-$ ,  $13/2^- \rightarrow 9/2^-$ , and  $15/2^- \rightarrow 11/2^-$  transitions.

With regard to strength functions it is interesting to consider average  $B(E2)$  values as a function of transition energy. Here, I will focus on the low-energy part of the distributions of  $\overline{B(E2)}$  values. As just discussed, the calculated  $B(E2)$  values of the low-energy transitions connecting many close-lying states with the dominating four-particle configuration  $\pi(0g_{9/2}^2)\nu(1d_{5/2}^2)$  are roughly reproduced in their magnitude and in particular the shape of the distributions at low transition energy below about 2 MeV is therefore considered realistic.

The  $\overline{B(E2)}$  values are shown in Fig. 5 for positive-parity states and in Fig. 6 for negative-parity states in  $^{94}\text{Mo}$ . For both parities, the  $\overline{B(E2)}$  values of stretched

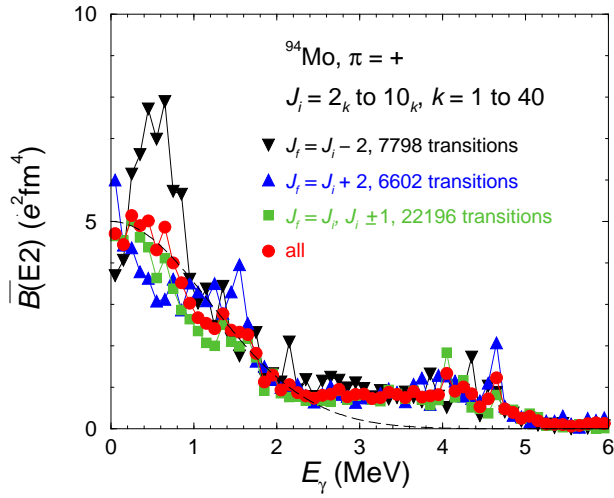


FIG. 5: (Color online) Average  $B(E2)$  values in 100 keV bins of transition energy calculated for positive-parity states in  $^{94}\text{Mo}$ . The black dashed curve is a Gauß curve with parameters given in the text.

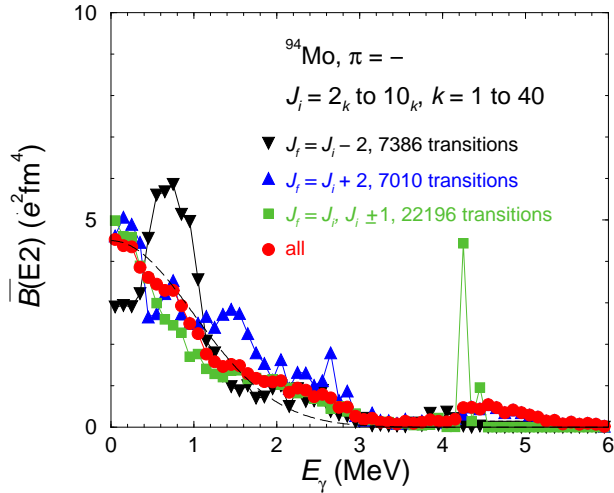


FIG. 6: (Color online) As Fig. 5, but for negative-parity states.

transitions with  $J_f = J_i - 2$  peak in the energy region between 0.4 and 1 MeV, whereas the  $\overline{B}(E2)$  values of the  $J_f = J_i + 2$  and  $J_f = J_i, J_i \pm 1$  increase with a slope getting gentle toward  $E_\gamma = 0$ . The decrease toward high energy is followed by peaks around 4.5 MeV for each parity. For positive-parity states shown in Fig. 5, the peak in the distribution of  $J_f = J_i - 2$  transitions arises from transitions depopulating high-lying  $2^+$  to the  $0_1^+$  and  $0_2^+$  states, high-lying  $4^+$  to the  $2_1^+$  and  $2_2^+$  states, and so on. The peak seen for  $J_f = J_i + 2$  transitions is caused by transitions from high-lying  $0^+$  to the  $2_1^+$  and  $2_2^+$  states. The  $\overline{B}(E2)$  values for  $J_f = J_i, J_i \pm 1$  transitions in the energy range between about 4 and 5 MeV belong to transitions from high-lying  $1^+$  and  $2^+$  states to the  $2_1^+$  and  $2_2^+$  states. For negative-parity states shown in Fig. 6,

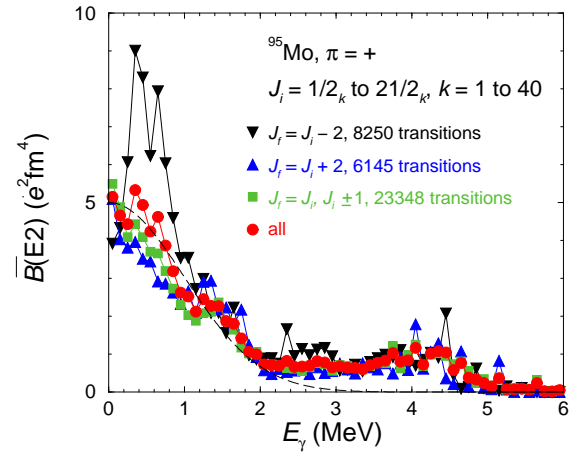


FIG. 7: (Color online) Average  $B(E2)$  values in 100 keV bins of transition energy calculated for positive-parity states in  $^{95}\text{Mo}$ . The black dashed curve is a Gauß curve with parameters given in the text.

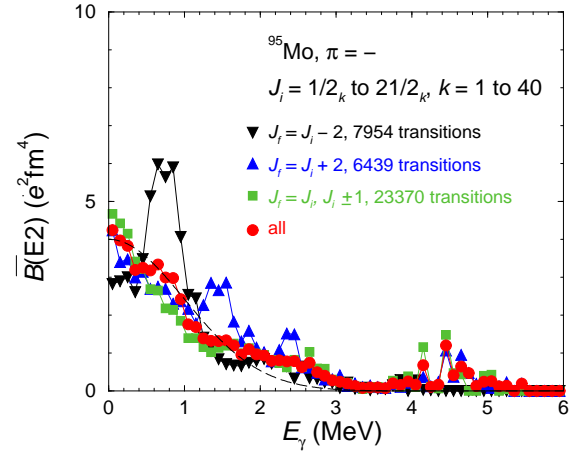


FIG. 8: (Color online) As Fig. 7, but for negative-parity states.

the peak in the distribution of  $J_f = J_i + 2$  states around 4.3 MeV is formed by transitions from high-lying  $0^-$  to the  $2_1^-$  and  $2_2^-$  states.

Also shown in Figs. 5 and 6 are the distributions including all transitions of positive and negative parity, respectively. These distributions are dominated by the behavior of the  $\overline{B}(E2)$  values of the  $J_f = J_i, J_i \pm 1$  transitions because of their large number. The bump in the distribution of the  $\overline{B}(E2)$  values of the  $J_f = J_i - 2$  transitions is averaged out, which again shows that in particular stretched  $E2$  transitions between slightly collective yrast states have a minor influence on the low-energy behavior of the  $E2$  strength functions. At energies below about 2 MeV, the  $\overline{B}(E2)$  distributions may be approximated by Gauß curves  $\overline{B}(E2) = B_0 \exp(-E_\gamma^2/2\sigma^2)$  with  $B_0 = 5.0 e^2\text{fm}^4$ ,  $\sigma = 1.2$  MeV for positive parity and  $B_0 = 4.5 e^2\text{fm}^4$ ,  $\sigma = 1.0$  MeV for negative parity.

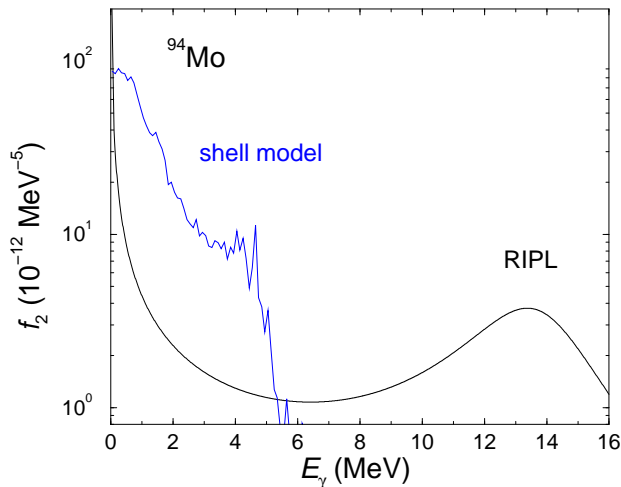


FIG. 9: (Color online)  $E2$  strength function for  $^{94}\text{Mo}$  deduced from the present shell model calculations (blue line) and the  $E2$  strength function according to the expression given in the RIPL handbook (black curve) [23].

The analogous plots for positive-parity states and negative-parity states in  $^{95}\text{Mo}$  are shown in Figs. 7 and 8, respectively. The distributions in this odd-mass  $N = 53$  nuclide look similar to the ones in the even-mass  $N = 52$  neighbor and are created by states analogous to the ones in  $^{94}\text{Mo}$ . The low-energy parts of the distributions of all transitions may be approximated by Gauß curves with parameters of  $B_0 = 5.0 e^2\text{fm}^4$ ,  $\sigma = 1.0$  MeV for positive parity and  $B_0 = 4.0 e^2\text{fm}^4$ ,  $\sigma = 1.0$  MeV for negative parity, which are very close to the corresponding values in  $^{94}\text{Mo}$ .

#### IV. $E2$ STRENGTH FUNCTIONS

$E2$  strength functions have been deduced from the  $\overline{B}(E2)$  distributions including all transitions in a way analogous to the one described in Ref. [20]. To calculate the  $E2$  strength function the relation  $f_2(E_\gamma) = 0.80632 \times 10^{-12} \overline{B}(E2, E_\gamma) \rho(E_i)$  was used, where  $\rho(E_i)$  is the level density in  $\text{MeV}^{-1}$  at the energy of the initial state. The  $f_2(E_\gamma)$  values were deduced in energy bins as done for the  $\overline{B}(E2)$  values. The level densities  $\rho(E_i, \pi)$  were determined by counting the calculated levels within energy intervals of 1 MeV for the two parities separately. The total level densities  $\rho(E_i)$  are well reproduced by the constant-temperature expression  $\rho(E_i) = \rho_0 \exp(E_i/T_\rho)$  for  $E_i < 5$  MeV. For higher energies the level density decreases with excitation energy, which is due to missing levels at high energy in the present configuration space and spin range. The parameters of the expression for  $\rho$  are  $\rho_0 = 1.37 \text{ MeV}^{-1}$ ,  $T_\rho = 0.67$  MeV for  $^{94}\text{Mo}$  and  $\rho_0 = 1.90 \text{ MeV}^{-1}$ ,  $T_\rho = 0.54$  for  $^{95}\text{Mo}$  [20].

The total  $E2$  strength functions for  $^{94}\text{Mo}$  and  $^{95}\text{Mo}$

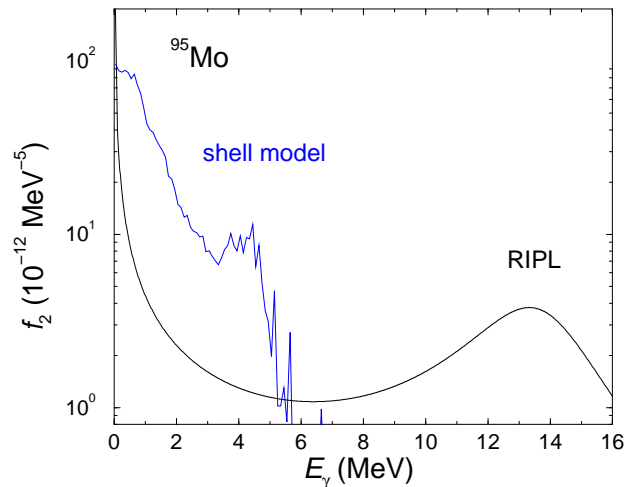


FIG. 10: (Color online) As Fig. 9, but for  $^{95}\text{Mo}$ .

are shown in Figs. 9 and 10, respectively. As seen for the  $\overline{B}(E2)$  distributions, the  $E2$  strength functions are bell-shaped at low energy below about 2 MeV. This is different from the low-energy energy behavior of the  $M1$  strength functions calculated within the shell model which steadily increase toward  $E_\gamma = 0$  [20].

For comparison, the curves calculated according to the phenomenological expression recommended in the RIPL handbook [23] for the  $E2$  strength function are plotted in Figs. 9 and 10. At  $E_\gamma = 0$  these curves have an unphysical pole in contrast to the finite maximum resulting from the present shell-model calculations. At medium energies the low-energy tails of the Lorentz curves underestimate the  $E2$  strength predicted in the shell-model calculations by more than one order of magnitude.

#### V. SUMMARY

A large number of  $E2$  transitions between excited states up to  $J = 10$  in  $^{94}\text{Mo}$  and  $^{95}\text{Mo}$  has been calculated using the shell model. At low transition energy below about 2 MeV, the distributions of average  $B(E2)$  values are dominated by the large number of transitions between states with  $J_f = J_i, J_i \pm 1$ . These are the transitions with large average  $B(M1)$  values discussed in Ref. [20]. The corresponding states contain large components of the configuration  $\pi(0g_{9/2}^2)\nu(1d_{5/2}^2)$ . The strength functions deduced from the average  $E2$  strengths increase toward zero transition energy and show a finite maximum of a Gauß-like shape. This is in contrast to the pole of the phenomenological expression recommended in the reaction data base RIPL. In the medium-energy range up to about 6 MeV the average  $E2$  strength predicted by the shell-model calculations shows a complicated structure and is by orders of magnitude greater than the low-energy tail of the phenomenological expression. This part may miss components caused by collective excitations

and may show a different behavior in nuclides that are more distant from shell closures than the ones studied in this work. The continuation of the strength to higher energy beyond about 6 MeV remains an open question. The possible influence of the low-energy shape of the  $E2$  strength functions on reaction rates may be tested by implementing these strength functions in statistical reaction codes.

## VI. ACKNOWLEDGMENTS

Helpful discussions with B. A. Brown and S. Frauendorf are gratefully acknowledged.

- 
- [1] M. Arnould *et al.*, Phys. Rep. **450**, 97 (2007).  
 [2] F. Käppeler *et al.*, Rev. Mod. Phys. **83**, 157 (2011).  
 [3] M. B. Chadwick. *et al.*, Nucl. Data Sheets **112**, 2887 (2011).  
 [4] S. Goriely, Phys. Lett. B **436**, 10 (1998).  
 [5] A. J. Koning, S. Hilaire, and M. C. Duijvestijn, AIP Conf. Proc. **769**, 1154 (2005).  
 [6] D. M. Brink, Ph. D. thesis, Oxford University, 1955, unpublished.  
 [7] P. Axel, Phys. Rev. **126**, 671 (1962).  
 [8] R. Capote *et al.*, Nucl. Data Sheets **110**, 3107 (2009).  
 [9] A. Bohr and B. R. Mottelson, *Nuclear structure, vol. II*, (W. A. Benjamin, Inc., Reading, Massachusetts, 1975).  
 [10] J. M. Eisenberg and W. Greiner, *Nuclear theory, vol. I*, (North-Holland, Amsterdam, 1975).  
 [11] A. R. Junghans *et al.*, Phys. Lett. B **670**, 200 (2008).  
 [12] J. Kopecky and M. Uhl, Phys. Rev. C **41**, 1941 (1990).  
 [13] K. Heyde, P. von Neumann-Cosel, and A. Richter, Rev. Mod. Phys. **82**, 2365 (2010).  
 [14] M. Guttormsen *et al.*, Phys. Rev. Lett. **109**, 162503 (2012).  
 [15] D. Savran, T. Aumann, and A. Zilges, Prog. Part. Nucl. Phys. **70**, 210 (2013).  
 [16] A. Voinov *et al.*, Phys. Rev. Lett. **93**, 142504 (2004).  
 [17] A. Voinov *et al.*, Phys. Rev. C **81**, 024319 (2010).  
 [18] M. Guttormsen *et al.*, Phys. Rev. C **71**, 044307 (2005).  
 [19] A. C. Larsen *et al.*, Phys. Rev. C **87**, 014319 (2013).  
 [20] R. Schwengner, S. Frauendorf, and A. C. Larsen, Phys. Rev. Lett. **111**, 232504 (2013).  
 [21] E. Litvinova and N. Belov, Phys. Rev. C **88**, 031302(R) (2013).  
 [22] T. von Egidy and D. Bucurescu, Phys. Rev. C **80**, 054310 (2009).  
 [23] T. Belgia *et al.*, *Handbook for calculations of nuclear reaction data, Reference Input Parameter Library-2*, Tech. Rep. IAEA-TECDOC-1506, International Atomic Energy Agency, Vienna, Austria, 2006 (see <https://www-nds.iaea.org/RIPL-2/>).  
 [24] D. Zwarts, Comput. Phys. Commun. **38**, 365 (1985).  
 [25] R. Schwengner *et al.*, Phys. Rev. C **80**, 044305 (2009).  
 [26] R. Schwengner *et al.*, Phys. Rev. C **66**, 024310 (2002).  
 [27] R. Schwengner *et al.*, Nucl. Phys. **A584**, 159 (1995).  
 [28] R. Schwengner *et al.*, Phys. Rev. C **57**, 2892 (1998).  
 [29] R. Schwengner *et al.*, Phys. Rev. C **74**, 034309 (2006).  
 [30] G. Winter *et al.*, Phys. Rev. C **48**, 1010 (1993).  
 [31] G. Winter *et al.*, Phys. Rev. C **49**, 2427 (1994).  
 [32] J. Reif *et al.*, Nucl. Phys. **A587**, 449 (1995).  
 [33] E. A. Stefanova *et al.*, Phys. Rev. C **62**, 054314 (2000).  
 [34] Y. H. Zhang *et al.*, Phys. Rev. C **70**, 024301 (2004).  
 [35] A. Jungclaus *et al.*, Nucl. Phys. **A637**, 346 (1998).  
 [36] A. Jungclaus *et al.*, Phys. Rev. C **60**, 014309 (1999).  
 [37] E. A. Stefanova *et al.*, Phys. Rev. C **63**, 064315 (2001).  
 [38] G. Rainovski *et al.*, Phys. Rev. C **65**, 044327 (2002).  
 [39] E. A. Stefanova *et al.*, Phys. Rev. C **65**, 034323 (2002).  
 [40] D. Abriola and A. A. Sonzogni, Nucl. Data Sheets **107**, 2423 (2006).  
 [41] S. K. Basu, G. Mukherjee, and A. A. Sonzogni, Nucl. Data Sheets **111**, 2555 (2010).